Proceedings World Geothermal Congress 2023
Beijing, China, April 17 – 21, 2023

The Role of Proppant on Hydraulic Permeability Enhancement of Fractured Granite Under Shear Stimulation

Qi Zhang[1], Jin Luo[1], Qi Zhao[2] and Jiale Zhang[1]

[1]Faculty of Engineering, China University of Geosciences (Wuhan); [2]Department of Civil and Environmental Engineering, The Hong Kong Polytechnic University,

E-mail address: qi_zhang1996@163.com; jinluo@cug.edu.cn; qi.qz.zhao@polyu.edu.hk; jialezhang2022@163.com

Keywords: Proppant; Shear stimulation; Hydraulic permeability; Fractured Granite; Fracture roughness

ABSTRACT

The fractures in a hot dry rock (HDR) reservoir are prone to be closed due to the high stress in the rock mass. Shear stimulation is considered an effective approach to enhance fracture openness through self-propping. On the other hand, proppants have been widely used to maintain fracture aperture after injections. However, the use of proppant in shear stimulation to improve the hydraulic permeability of an HDR reservoir is insufficiently investigated. To understand the evolution of hydraulic permeability, shear tests are implemented on raw fracture and propped fracture with the grain size of P0.1, P0.5 and P1.0. The monitoring of vertical displacement shows a shear dilation, meaning an increase of the fracture aperture. The larger the grain size the larger the changing of vertical displacement is, meaning the higher enhancement of hydraulic conductivity. The hydraulic conductivity of fractures is maximally increased by 1600 times when using proppants with the grain size of P1.0 compared with the unpropped sample. Furthermore, the 3D morphological analysis shows the proppant reduces shearing damage and protects effectively the fracture roughness, which in turn enhances the effects of shear stimulation on the hydraulic conductivity of the fracture. Conclusively, the placing of proppants in a shear stimulation can improve the hydraulic permeability of fracture effectively by propping effects and by maintaining the roughness of fracture.

1. INTRODUCTION

The hot dry rock (HDR) mass in its natural state is often low-porous and low-permeable, and the huge energy contained in it cannot be effectively used for a long time without reasonable engineering stimulation (Zhu et al., 2015; Sun et al., 2017; Lu, 2018). To exploit the geothermal energy in HDR reservoirs, Enhanced Geothermal System (EGS) was proposed by stimulating the permeability through hydraulic fracturing (Luo et al., 2018; Chen & Jiang, 2015; Huang et al., 2020). In the EGS, an injection well is first drilled in a reservoir. A sufficiently high water pressure is used to inject water into the well, and to create new fractures and reactivate the pre-existing fractures to generate a fractures network with enhanced permeability. Two or more pumping wells are drilled into the activated fracture network to form a flow channel for water circulation (Zhu et al., 2016; Zeng et al., 2013; Olasolo et al., 2016). Hence, many underground engineering problems and engineering geological problems caused by the resurrection of faults or cracks during stimulation need to be addressed during the construction of EGS.

Proppants, typically high-strength granular materials, are often injected into the reservoir accompanied by fracturing fluids to maintain permeability after hydraulic fracturing (Gong et al., 2020; Aslannezhad et al., 2021). Until now, proppant is an important material used in the petroleum industry, mainly for improving recovery from oil and gas reservoirs (Chen et al., 2021; Tan et al., 2018). Although numerous studies have been performed to investigate the use of proppant in oil/gas reservoirs, experimental studies on the use of proppant in HDR is insufficiently. Moreover, previous studies mainly focused on the point of proppant embedment (Wang et al., 2020; Zhong et al., 2019) and migration (Isah et al., 2021; Barboza et al., 2021) in fractures. The existence of proppant makes the conductive capability in fractured rock mass difficult to predict. The role of proppant in fracture damage evolution in hard rock needs to be revealed.

Shear stimulation, also called hydro shearing or shear-dilation-based hydraulic stimulation, is believed to reactivate preexisting fractures by pressurized fluid injection, causing them to slip and dilate for permeability enhancement of HDR reservoirs (Ghassemi, 2012; Ye & Ghassemi, 2018; Bijay & Ehsan, 2021). Guglielmi et al. completed two mesoscale reactivation tests by injecting high-pressure fluid into a carbonate fault (Guglielmi, Cappa, et al., 2015) and a shale fault (Guglielmi, Elsworth, et al., 2015), respectively. One of the insights achieved from these two in situ reactivation tests is that aseismic/seismic shear slip by fluid injection enhanced the fluid conductivity of the faults. In contrast to hydraulic fracturing in the petroleum industry which involves massive high-pressure injection and proppant use, some researchers argue that an EGS stimulation should be carried out at treatment pressures below the minimum principal stress and fracture self-propping by asperities is viewed as an effective means of flow rate retention (Ye & Ghassemi, 2018b; Huang et al., 2013). Although shear stimulation is successfully applied in several HDR reservoirs, the micro-mechanical mechanism of propped fractures has not been studied and analyzed in detail.

Although the aforementioned process of shear stimulation is theoretically well understood and routinely modeled, the experimental studies on the hydraulic property were insufficient (Hofmann et al., 2016; Ishibashi et al., 2016; Vogler et al., 2016). In this study, the deformation characteristics (shear dilation) and fluid flow parameters (hydraulic conductivity and equivalent hydraulic aperture) of the fractures with different surface roughness are measured to examine the following key points: (1) the evolution of fluid flow parameters under different proppant conditions, (2) the mechanisms of permeability enhancement of propped granite in shear process, and (3) shear-induced roughness degradation and the influence of proppants on the hydraulic conductivity and dilatancy characteristics of fracture in the shearing process.

2. MATERIAL AND METHODS

2.1 Specimen Preparation

The rock samples are collected from an outcrop of the rock formation of a geothermal site located in the Gonghe basin of Qinghai province, China. The density of rock is 2.62 - 2.65 g/cm^3. The granite mainly consists of quartz (20% - 30%), plagioclase (25% - 35%), alkaline feldspar (30% - 38%) and mica (5% - 7%). The rock samples are cut into 100 mm sized cubes and cylindrical granite samples with 50-mm-diameter, and then split into two equal sized halves using an indirect tensile test setup. This created matching rough fractures that we examined in this study. Three sets of quartz sand with different grain size ranges (0.1-0.5 mm, 0.5-1.0 mm, and 1.0-2.0 mm) are used as proppant (Fig. 1a). The four proppant conditions (no proppant and three abovementioned proppant samples, referred to as P0.0, P0.1, P0.5, and P1.0, respectively) are studied. 16 samples are prepared for the direct shear test and 1 sample is prepared for hydraulic properties test, and they are tested as described in the following sections. Fig. 1b shows the placement and distribution of proppant in the rough surface of a fracture. For each size, the proppants are placed on the fracture surface with an average thickness as possible. A portion of the proppants are concentrated in low-lying areas and few proppants are stagnant due to the asperity of the fracture, as shown in Fig. 1b.

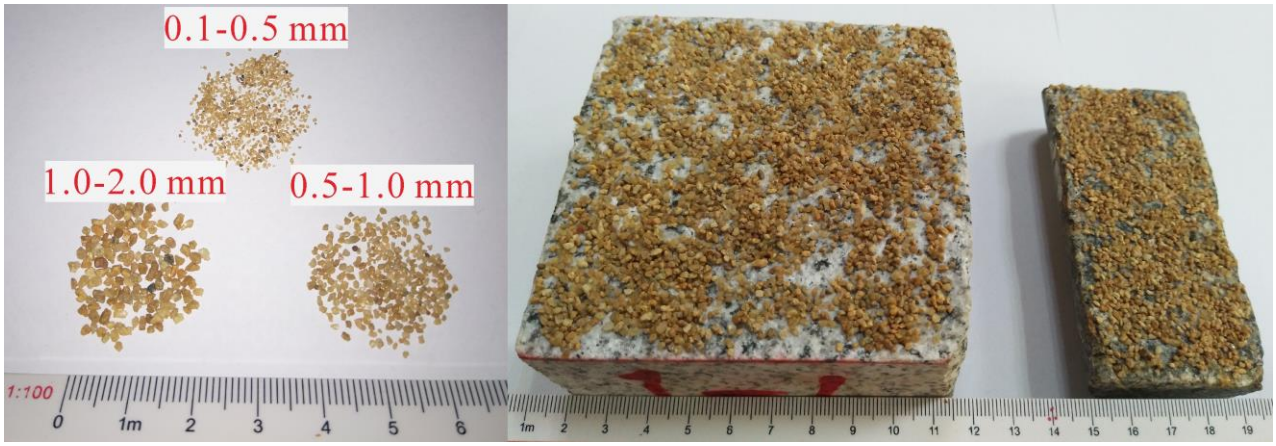

Figure 1: The preparation of the fractured granite with proppant for shearing tests and hydraulic conductivity tests. (Left: Proppant with 3 common grain sizes; Right: Placement of the proppant on the fracture surface).

2.2 Quantitative evaluation of fracture surface roughness

The rapidly developed three-dimensional (3D) scanning technology is an effective tool for reconstructing and analyzing the morphology of a fracture surface. The dense point cloud with spatial coordinate information of the fracture surface can be obtained quickly and non-destructively with high precision by scanning. The reconstruction technique can then be used to digitize the fracture surface and import it into a computer for processing and evaluating the roughness degradation or damage state of the fracture surface during the direct shear test.

Three-dimensional (3D) digitization of the joint surfaces is acquired by the 3D CaMega scanner (Fig 2a), which has a 30 μm spatial resolution, and we subsample the point cloud into a 50 μm resolution uniform grid mesh. We extract 2D profiles along the shear direction at 0.4 mm separation for roughness analysis. The plane is transformed so that the mean plane is flat for further analysis. To avoid the influence of chipping at edges, the 5 mm margin data points are discarded in further analysis. The roughness of all joints is examined before and after the tests. Various methods are used to evaluate the rock joint roughness (Magsipoc et al., 2020).

Joint Roughness Coefficient (JRC) is commonly used to estimate the roughness of a fracture. JRC evaluation is performed on profiles consisting of equally spaced nodes, and for a rough surface, equally spaced profiles are usually obtained in the direction parallel to the shearing direction, as shown in Fig. 2. In the previous studies, Tse and Cruden (1979) established correlations between JRC and Z_2 (the root mean square of the first deviation of the profile) proposed by Myers (1962) and the structure function (SF) by Sayles and Thomas (1977). Yang et al. (2001) reconstructed the ten standard profiles utilizing the Fourier transform and updated the correlations between JRC and Z_2 as well as SF. JRC is related to the Z_2 parameter that reflects the fluctuation of the rough surface as follows:

$$Z_2 = \left[\frac{1}{L}\int_{x=0}^{x=L}\left(\frac{dy}{dx}\right)^2 dx\right]^{1/2} = \left[\frac{1}{L}\sum_{i=1}^{i=N-1}\frac{(y_{i+1}-y_i)^2}{x_{i+1}-x_i}\right]^{1/2} \quad (1)$$

$$SF = \frac{1}{L}\int_{x=0}^{x=L}[f(x+dx)-f(x)]^2\,dx = \frac{1}{L}\sum_{i=1}^{i=N-1}(y_{i+1}-y_i)^2(x_{i+1}-x_i) \quad (2)$$

where N is the number of evenly spaced sampling points, x_i and y_i are the x and y coordinates for the i_{th} point.

In this study, the JRC_i of the i_{th} profile is calculated by the following equation (Tse and Cruden, 1979; Yang et al., 2001):

$$JRC = 32.2 + 32.47\lg(Z_2) \quad (3)$$

$$JRC = 37.63 + 16.5\lg(SF) \quad (4)$$

In order to obtain a representative JRC value of the fracture surface, the surface profiles are parallel extracted with an internal 0.4 mm along the shear direction, as shown in Fig. 2. The JRC of the extracted profiles are estimated by Eq. (1-4). Then, the JRC of the fracture surface is estimated by considering the mean value of all the profiles by following Eq. (5):

$$\mathrm{JRC_s} = \frac{\sum_i^n JRC_i}{N} \tag{5}$$

where $\mathrm{JRC_s}$ is the Joint Roughness Coefficient (JRC) of the fracture surface, $\mathrm{JRC_i}$ is the roughness index of the extracted profile i, N is the number of the created profile of the fracture surface to estimate the JRC values.

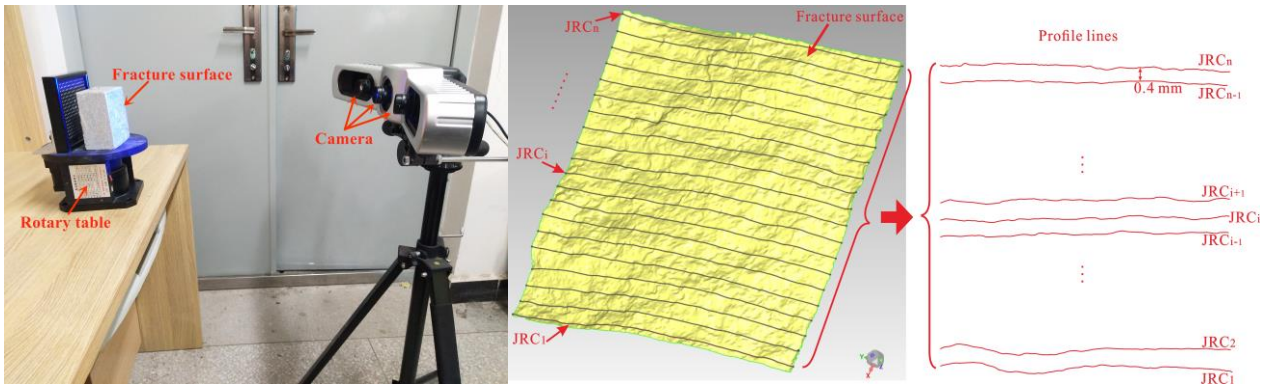

Figure 2: (a) Three-dimensional scanning of the fracture surface for the characterization of morphological information before and after the shear tests. (b) Estimation of the surface Joint Roughness parameters.

2.3 Direct shear test

To better understand the effects of proppant on hydro-shear behavior under different stress conditions, direct shear tests are conducted. The experiments are conducted using the RMT150C testing apparatus (Fig. 3) at the Institute of Rock and Soil Mechanics, Chinese Academy of Sciences, Wuhan, China. The tests are servo-controlled, and the normal load and tangential load are applied to the shear box through a hydraulic jack. To ensure that the load is uniformly distributed on the specimen, steel plates with steel balls are installed to transfer the load on the vertical and horizontal sides of the specimen evenly. The rock sample is placed in a shear box in which the lower part is fixed, and the upper part is moved at a constant rate of 0.01 mm/s. In this study, a 50 kN vertical pre-load is first applied to the rock sample and lasted for 10 min before the start of the shear test to fully close the fractures. Normal loads of 10 kN, 20 kN, 30 kN and 40 kN (equivalent of 2 MPa, 3 MPa, 4 MPa, and 5 MPa nominal normal stress) that remained constant during shear are applied, as shown in Table 2. During the test, the dilatancy displacement is collected by a displacement sensor at the top of the specimen.

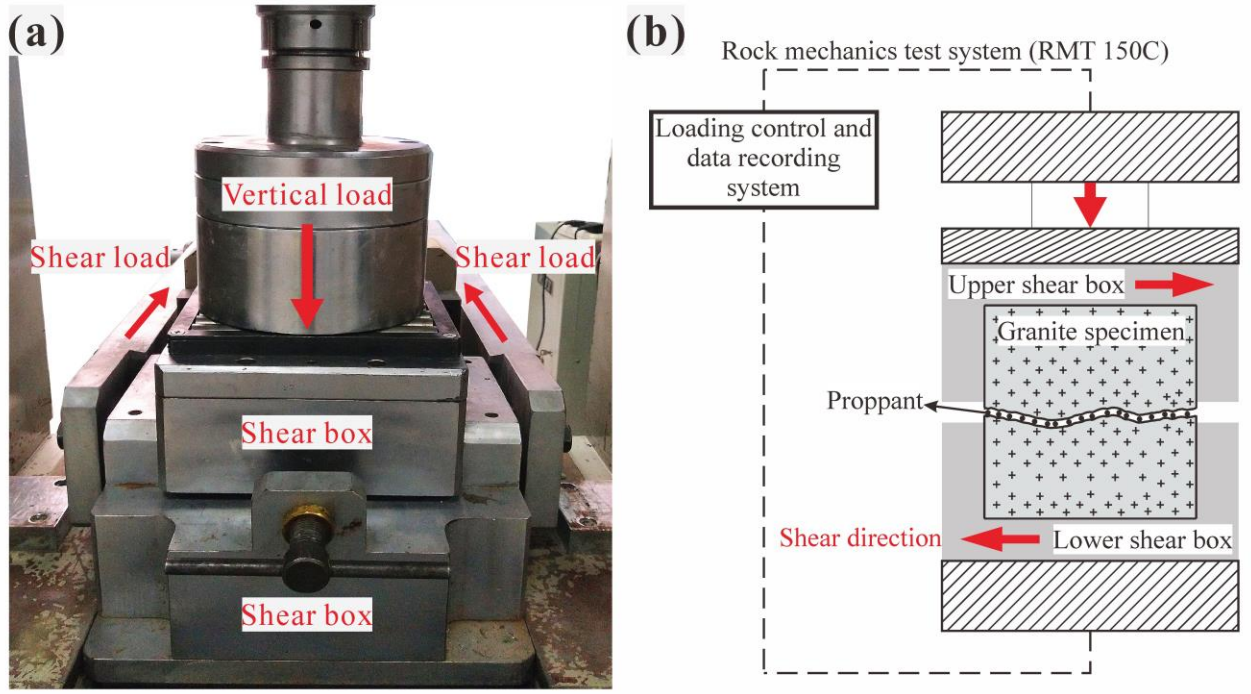

Figure 3: (a) RMT 150 rock mechanics test apparatus and (b) shear schematic diagram.

2.4 Permeability Evaluation

To study the hydraulic properties of fractured granite samples under coupled hydro-mechanical conditions, one granite sample is prepared to investigate the hydraulic properties under different proppant conditions as shown in Table 1.

Table 1 Setting and grouping of hydraulic permeability test

Proppant condition (mm)	Confining pressure (MPa)	Pore pressure (MPa)
P 0.0 (No prppant)	0.4	0.1 - 0.2 - 0.3
	0.8	0.1 - 0.2 - 0.3
	1.2	0.1 - 0.2 - 0.3
P 0.1 (0.1-0.5 mm)	0.4	0.1 - 0.2 - 0.3
	0.8	0.1 - 0.2 - 0.3
	1.2	0.1 - 0.2 - 0.3
P 0.5 (0.5-1.0 mm)	0.4	0.1 - 0.2 - 0.3
	0.8	0.1 - 0.2 - 0.3
	1.2	0.1 - 0.2 - 0.3
P 1.0 (1.0-2.0 mm)	0.4	0.1 - 0.2 - 0.3
	0.8	0.1 - 0.2 - 0.3
	1.2	0.1 - 0.2 - 0.3

The testing system consisted of an air compressor, pressure control units, confining chamber, an electronic scale, and a computer, as shown in Fig. 4. Within the testing system, the hydraulic properties of the fractured samples under coupled hydro-thermal-mechanical conditions can be studied. The instrument can apply pore pressures varying from 0 to 1 MPa and confining pressures ranging from 0 to 5 MPa with an accuracy of ± 0.25%. The diameter of the samples is limited to a maximum of 50 mm. The confining pressure, fluid temperature and flow rate, are automatically recorded with a data acquisition system. The procedure for the tests is as follows:

(1) A single fracture is created in a granite specimen using the indirect tensile splitting method. The fracture penetrates through the center of the speciemn parallel to the axial direction. To avoid the influence of roughness on the fluid flow and proppant movement, all the tests are implemented in the same fractured granite sample and the same injection direction.

(2) Three sets of quartz sand with different grain size ranges (P0.1, P0.5 and P1.0) are placed evenly on the fracture surface with a mean density of 10/cm^2 and sandwiched evenly between the two halves of the specimen. Then, the sample assembly is covered by an elastic latex membrane. To prevent the latex membrane from rupturing due to pressure difference, waterproof tape and Ethylene Viny Acetate (EVA) hot melt adhesive are used to fix fractured granite with proppant, which also prevents the proppant from moving during sample loading. Meanwhile, hot melt adhesive is used to seal both sides of the fracture to make water flow only along the inside of the fracture.

(3) The sample is mounted into the testing instrument, as shown in Fig 5. The confining pressure is set firstly as Table 1 at room temperature (26 ℃). When the confining pressure is stable, the pore pressure is then increased with a incremental step of 100 kPa - 200 kPa - 300 kPa, and the the flow rate, confining pressure and pore pressure during the testing are recorded. The sample is mounted vertically in the instrument and the pore fluid is pumped from the bottom to the top to force air out. To remain a steady confining pressure, 10 minutes are waited before applying the pore pressure. Afterwards, to achieve a stable flow rate, the fluid flowing tests are conducted for a duration of 10 minutes. During the experiments, data including inlet and outlet flow rate and pressures are continuously recorded by a data logger. In the test, we ensure that the pore pressure is lower than the confining pressure by at least 0.1MPa.

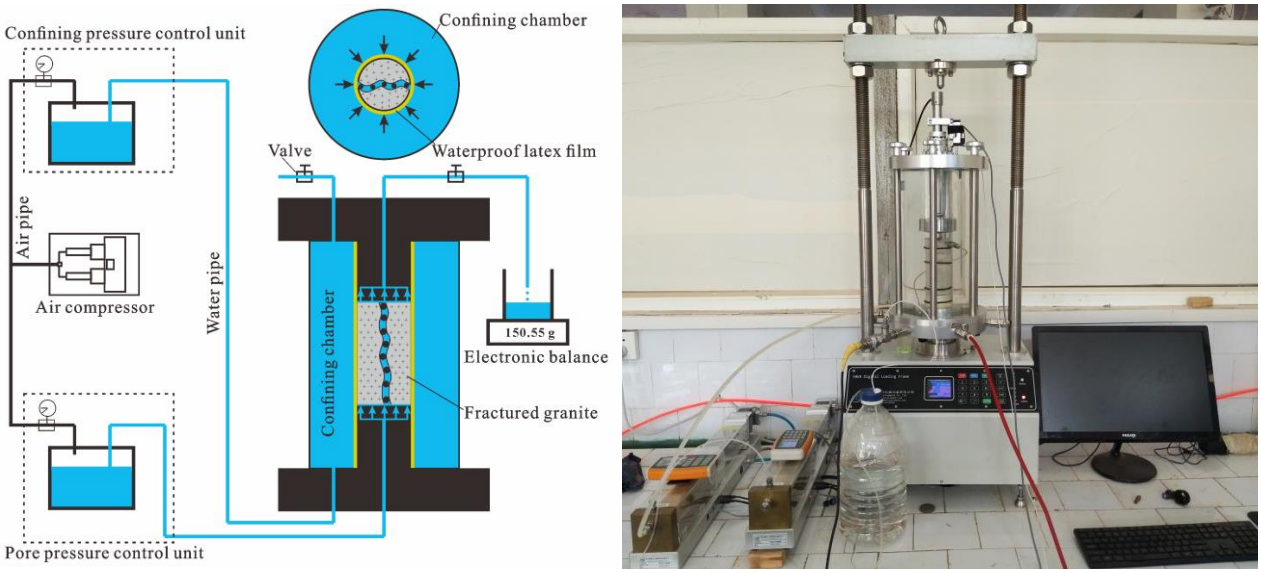

Figure 4: (a) Schematic and (b) object pictures of experimental arrangement for the measurement of the evolution of permeability. Confining pressure control unit controls the confining pressure applied across the fracture. Pore pressure control unit injects the fluid at a prescribed flow rate or pressure, allowing the fluid flow along the fractures.

For rock samples with a single fracture, hydraulic conductivity can be determined by the fracture aperture (Liu, 1987; Xiong et al., 2009). The size of the hydraulic aperture of each fracture is calculated by following the cubic law for fluid flow in a single-fracture rock mass (Witherspoon et al., 1980). By considering the fluid viscosity, fluid flow rate and hydraulic gradient, the fracture aperture can be expressed as follows:

$$e = \left(\frac{12qv}{gJ_f}\right)^{\frac{1}{3}} \tag{6}$$

where e represents the size of the fracture aperture (m), q represents the flow rate per unit width of the fracture (m^2/s), v represents the kinematic viscosity coefficient of fluid ($g/m^2.\ s^2$), J_f represents the hydraulic gradient in the fracture (-), and g represents the gravitational acceleration (m/s^2).

Based on Equation (6), the hydraulic conductivity coefficient can be further determined according to the following equation:

$$K_j = \frac{ge^2}{12v} \tag{7}$$

where K_j represents the hydraulic conductivity (Wang, 2002; Tsang & Witherspoon, 1983).

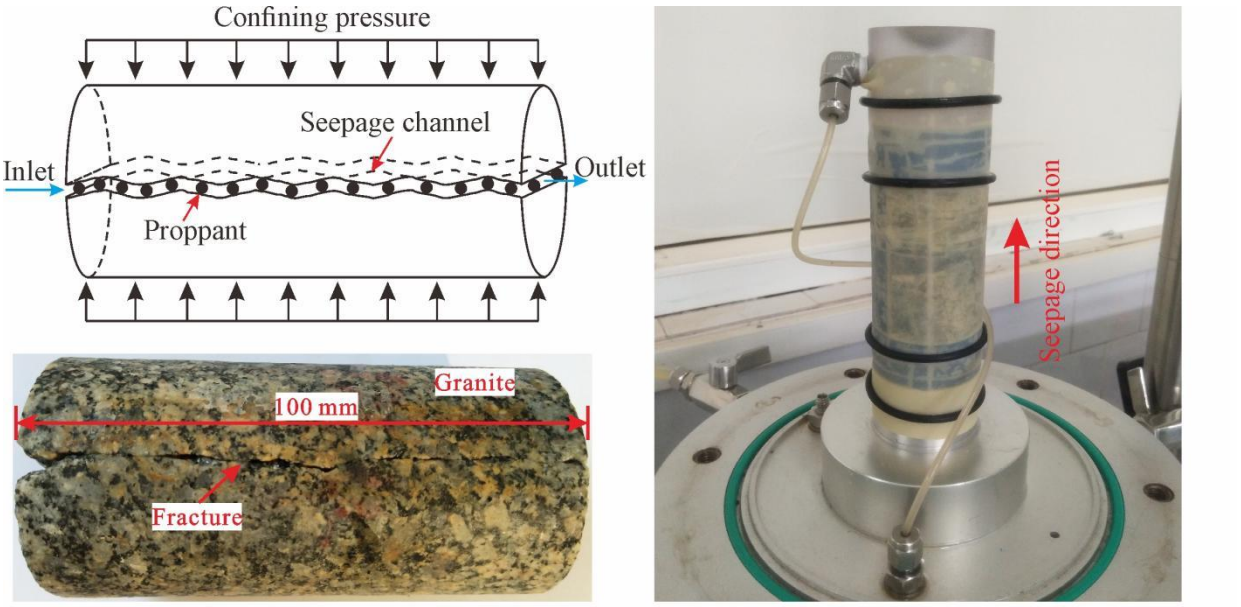

Figure 5: Sketch of the testing setup including (a) fully fitted fractured granite, and (b) the rock specimen encapsulated with latex film on the injection instrument.

3. RESULTS

3.1 The hydraulic properties of fractured granite with proppant

To investigate the effects of proppant on hydraulic properties, the test is executed under constant confining pressure and pore pressure. Hydraulic parameters such as fracture hydraulic aperture and hydraulic conductivity are investigated by changing the proppant conditions. The equivalent hydraulic aperture and hydraulic conductivity of fracture are determined using Equation (6-7), and the results are shown in Fig. 6.

It can be seen from Fig. 6 that the equivalent hydraulic aperture and hydraulic conductivity of the injecting system composed of granite rough fractures and proppant increase with the increase of proppant grain size. The equivalent hydraulic aperture increases from 119.79 μm to 1192.07 μm and the average hydraulic conductivity increases by 6.78-90.64 times from 0.013 mm/s to 1.150 mm/s. It can be seen that, due to the large opening of the fractures in the granite containing proppant and the large number of pores between the proppants, the proppant can play a role in promoting fluid flow in the fracture and hydraulic conductivity is 2 orders of magnitude higher than that of rough fractures without proppant. In addition, the permeability of fractures under the conditions of P0.0 and P0.1 decreases with the increase of confining pressure while the rule no longer appears under the condition of P0.5 and P1.0. It means that the proppant of P0.5 and P1.0 has a better supporting role and offsets the role of confining pressure.

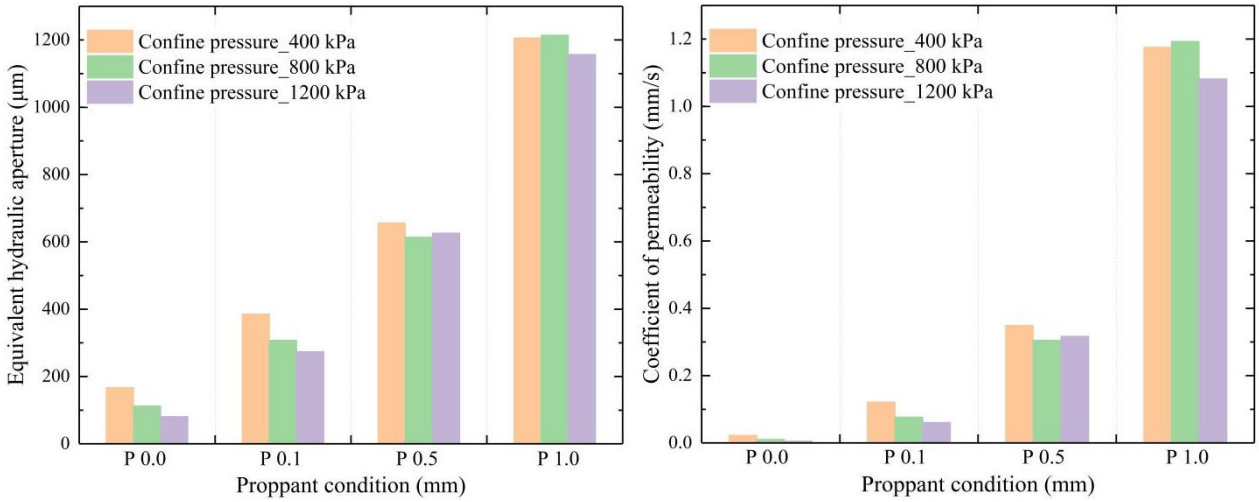

Fig. 6 The changing of the permeability of fractures under four proppant conditions

Previous studies have demonstrated that hydraulic conductivity is found to decrease with increasing confining pressure (Luo et al., 2017). The same phenomenon is observed under the condition of P0.0 and P0.1 in this study. Similar to fracture aperture, hydraulic conductivity is also found to decrease with increasing confining pressure. Hydraulic conductivity depends mainly on the fracture aperture size, and hence a similar decreasing trend is observed between the hydraulic conductivity and the confining pressure. However, in the condition of P0.5 and P1.0, the hydraulic permeability of propped fracture is no longer controlled by confining pressure under the same proppant condition and pore pressure.

3.2 The degradation of roughness during shear

According to the result calculated by Equation (1-5), the variation of surface roughness due to the shear deformation showed a clear correlation with proppant conditions. The estimated surface roughness values including SF and Z_2 before and after the shear tests are demonstrated in Table 2. The mean value of △JRC for the four proppant conditions (P0.0, P0.1, P0.5, and P1.0) are -11.36, -4.75, -1.47, and -3.19, respectively. The JRC values decreased drastically in the samples without placing proppant, implying a roughness degradation in the shearing test, as shown in Fig. 7. Meanwhile, the reduction of JRC becomes slighter by an average of 3.14 in the samples with proppants. These findings indicate that surface asperity is effectively protected by proppant.

Table 2 Surface roughness values measured both before and after the direct shear test

No	Proppant conditions (mm)	Vertical load (kN)	Part	Before Shear		After Shear	
				SF	Z_2	SF	Z_2
1-1	P0.0	10	Upper	0.0848	0.4068	0.0159	0.1732
			Lower	0.0317	0.2461	0.0115	0.1464
1-2		20	Upper	0.0440	0.2918	0.0079	0.1302
			Lower	0.0170	0.1793	0.0073	0.1251
1-3		30	Upper	0.0777	0.3890	0.0077	0.1290
			Lower	0.0846	0.4064	0.0054	0.1046
1-4		40	Upper	0.0675	0.3619	0.0073	0.1163
			Lower	0.0097	0.1346	0.0068	0.1117

2-1	P0.1	10	Upper	0.0136	0.1605	0.0151	0.1682
			Lower	0.0095	0.1337	0.0057	0.1025
2-2		20	Upper	0.0153	0.1696	0.0110	0.1436
			Lower	0.0163	0.1758	0.0127	0.1544
2-3		30	Upper	0.0271	0.2270	0.0115	0.1468
			Lower	0.0200	0.1966	0.0076	0.1185
2-4		40	Upper	0.0104	0.1505	0.0311	0.2628
			Lower	0.0065	0.1182	0.0255	0.2377
3-1	P0.5	10	Upper	0.0163	0.1762	0.0175	0.1816
			Lower	0.0341	0.2554	0.0122	0.1514
3-2		20	Upper	0.0143	0.1644	0.0272	0.2444
			Lower	0.0079	0.1215	0.0069	0.1129
3-3		30	Upper	0.0224	0.2059	0.0172	0.1801
			Lower	0.0655	0.3567	0.0403	0.2780
3-4		40	Upper	0.0081	0.1240	0.0067	0.1112
			Lower	0.0112	0.1454	0.0085	0.1253
4-1	P1.0	10	Upper	0.0149	0.1675	0.0125	0.1532
			Lower	0.0177	0.1825	0.0177	0.1825
4-2		20	Upper	0.0554	0.3273	0.0285	0.2330
			Lower	0.0319	0.2476	0.0138	0.1609
4-3		30	Upper	0.0148	0.1674	0.0178	0.1831
			Lower	0.0158	0.1729	0.0202	0.1957
4-4		40	Upper	0.0280	0.2323	0.0153	0.1698
			Lower	0.0420	0.2842	0.0077	0.1198

The roughness of fracture surfaces decreases after the shear test, and the existence of proppant alleviates the degradation degree of the fracture surface. It implies that the presence of proppant reduces the occurrence of asperity failure events and promotes the occurrence of the self-supporting dilatancy effect of rough fracture in the shear process. Moreover, the results also indicated that the small grain size proppant readily filled the valleys of small-scale roughness while larger grains tended to engage with asperities causing stress concentration that eventually crush the proppant grains.

It is worth mentioning that, unlike the overall trend, the JRC of No.2-4&4-4 change more than others under P0.1 and P1.0. It can be attributed to the higher normal stress (5MPa) and the anisotropy of fracture surface roughness. Besides, the JRC of No.3-2&4-3 increased slightly after the shear test. It reveals the complexity of the roughness degradation process in the presence of proppants.

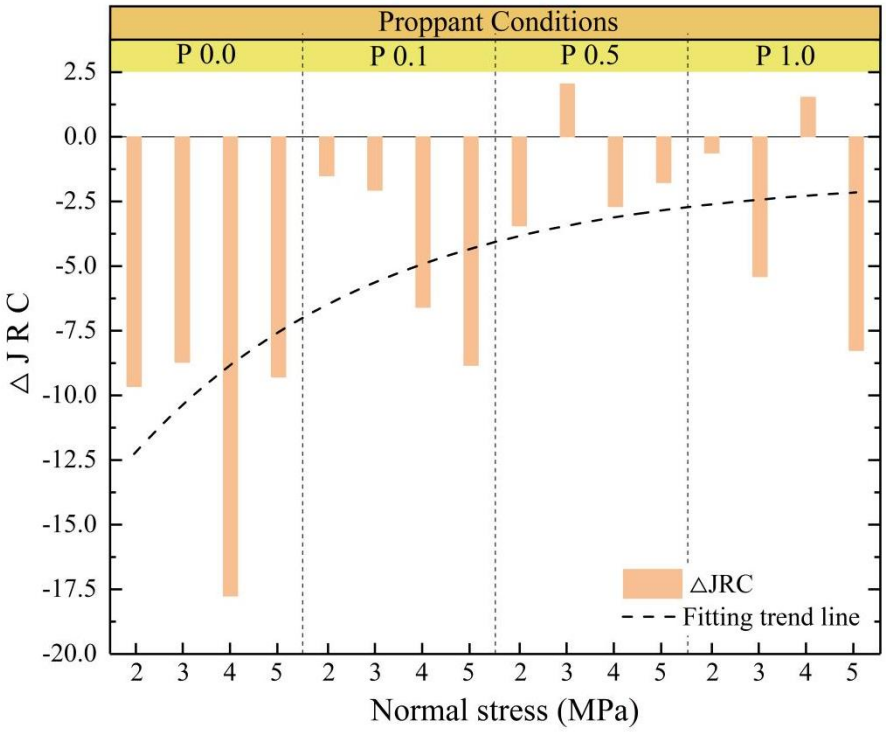

Fig. 7 The changing of the estimated Joint Roughness Coefficient (JRC) of fracture surfaces before and after the shear tests

3.3 Shear dilation and equivalent hydraulic aperture

In the typical direct shear experiment, the vertical displacement experienced a transition from compaction to dilation with increased shear displacement. Most observations followed this general trend (Shi et al., 2017), but the forms of the dilation curves under propped conditions are altered, as shown in Fig. 8. Overall, experiments with low vertical load had higher dilation values than those under high vertical load. Compared with the non-proppant condition, the curve under the supported condition has a shear slide phase and lower final dilatancy value. The larger the proppant grain size, the more significant the shear slide phase, with correspondingly less dilation. During the shearing process, the vertical displacement of the non-proppant condition is all more than 1.5 mm. The dilation effect with a longer shear slip distance is significantly alleviated in the fracture by proppant placement and that can reach down to 0.37 mm.

The shear dilation effect of the four suites of direct shear test can be described with linear displacement envelopes, where the k is the slope of vertical displacement curve in the dilatancy stage that describes the rate that fracture aperture increases with the shear process. The mean final dilatancy value for the four sets of experiments with different proppant conditions (P0.0, P0.1, P0.5, and P1.0) are 1.87 mm, 1.33 mm, 1.26 mm, and 0.74 mm, respectively; and the mean k values are 0.123, 0.093, 0.117, and 0.075, respectively. In addition, the shear sliding distance before dilatancy under conditions of P0.5(blue) and P1.0(magenta) is obviously longer than that under conditions of P0.0(black) and P0.1(red), as shown in Fig. 8. With the introduction of the proppant, the final dilatancy value at 15 mm of shear displacement and the dilatancy rate are all reduced with increasing proppant grain size. It means that the proppant can play a lubricating action in the shear process of rough fractures. Based on the above analysis of roughness, it can be concluded that the flattened linear dilatancy envelopes under propped conditions, together with injection fluid pressure in situ, would render the stimulated fractures more susceptible to shear slip, which is instructive to the enhancement of hydraulic conductivity.

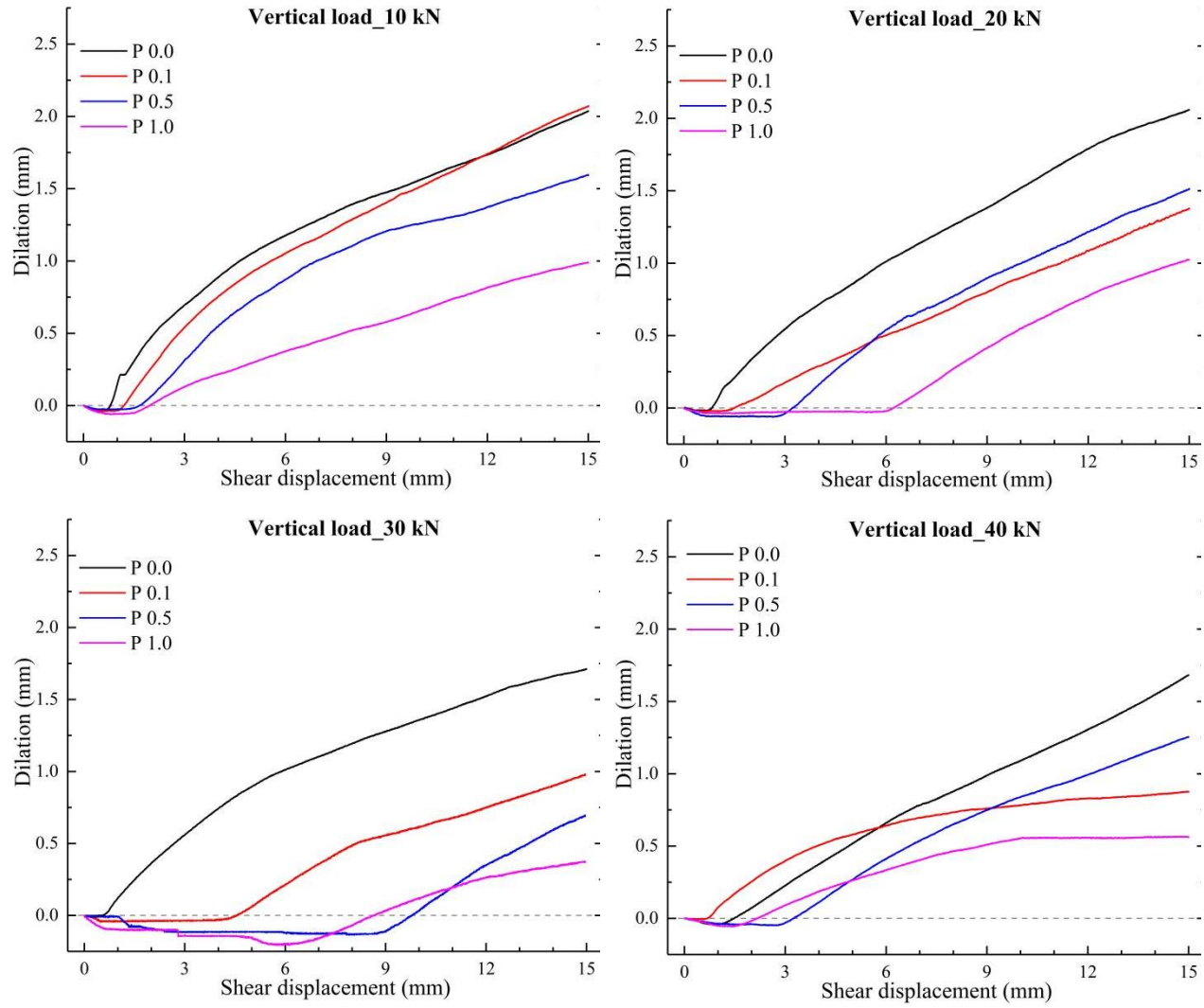

Figure 8: The vertical displacement during the shearing process indicating a dilation effect

To verify accurately the improvement of proppant on the hydraulic conductivity of fractures, the hydraulic aperture of the propped fractures is calculated by empirical relation. The calculation method of the initial mechanical opening E_i of the fracture is calculated by the size of the granite, as shown in Fig. 9. Firstly, the height of the rock sample is measured by a micrometer before and after the granite splitting. The difference in size is used as the mechanical opening of the fracture before the vertical pre-load is applied, and the closure of the fracture after the vertical load is subtracted. The proppant grain size is cumulated as the initial mechanical opening Ei before the shear began. The hydraulic opening before and after shearing are calculated respectively, and $\triangle E_d$ adopts the vertical displacement variation of the fracture shear process.

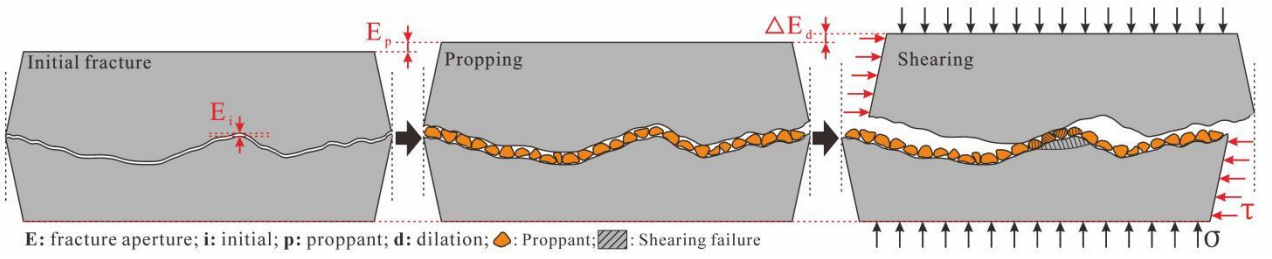

Figure 9: Calculation process of the equivalent hydraulic aperture of propped granite fractures during shear tests

The measurement of hydraulic aperture (e) is a complicated task. In this study, we adopt the empirical relation of (Olssona & Barton, 2001)

$$e = \frac{E^2}{\mathrm{JRC}^{2.5}}, E \geq e_{\mathrm{h}} \tag{6}$$

where E is the mechanical aperture calculated as:

$$E = E_{\mathrm{i}} + E_p + \Delta E_{\mathrm{d}} \tag{7}$$

where E_i is the initial mechanical aperture, E_p is the grain size of the proppant, and ΔE_d is the shear-induced mechanical aperture change which is determined by dilation displacement during the direct shear test.

The improvement of the hydraulic conductivity is estimated by considering the cubic law and the shear dilation effects. According to the calculation results, it can be found that the joint influence of proppant and shear dilatancy can increase the hydraulic aperture of the fracture by two orders of magnitude at least, and the maximum increase ratio can reach more than 1600 times compared with that before shear stimulation, as shown in Table 3. When the fracture is in a pure shear state, the self-supporting effect of asperities increases the hydraulic aperture by 79 to 281 times. With the propped conditions, the enhancement multiple of the hydraulic aperture of the propped fractures increases with the increase of proppant grain sizes, which is not inherently related to vertical load. It can be concluded that the presence of shear sliding, regardless of loading conditions and proppant conditions, increases the hydraulic permeability of fractures.

Table 3 The changing of the hydraulic aperture of the propped fractures before and after the shearing stimulation

Proppant size (mm)	Vertical load (kN)	E_i (mm)	$\triangle E_d$ (mm)	E (mm)	e_{before} (mm)	e_{after} (mm)	Increased multiple (After/before)	
P 0.0	10	0.13	1.46	1.59	1.60E-05	2.39E-03	150	179
	20	0.15	1.36	1.51	1.76E-05	4.95E-03	281	
	30	0.09	1.24	1.33	1.36E-05	1.07E-03	79	
	40	0.11	1.04	1.15	1.55E-05	3.20E-03	207	
P 0.1	10	0.09	1.43	1.62	3.41E-04	3.98E-02	117	195
	20	0.08	0.85	1.03	3.93E-05	6.52E-03	166	
	30	0.10	0.79	0.99	1.01E-05	2.75E-03	272	
	40	0.05	0.75	0.9	1.56E-04	3.50E-02	225	
P 0.5	10	0.15	1.24	1.89	2.24E-05	9.88E-03	441	249
	20	0.06	1.13	1.69	1.94E-04	5.54E-02	286	
	30	0.13	0.69	1.32	2.30E-05	2.37E-03	103	
	40	0.12	0.93	1.55	4.23E-04	7.06E-02	167	
P 1.0	10	0.08	0.65	1.73	6.99E-05	1.73E-02	247	546
	20	0.06	0.96	2.02	3.02E-06	4.92E-03	1632	
	30	0.12	0.53	1.65	9.51E-05	1.80E-02	189	
	40	0.16	0.55	1.71	4.01E-05	4.58E-03	114	

3.4 The fracture hydraulic properties under proppant accumulation

In previous numerical studies, it has been proved that proppant accumulation in fracturing fracture, which usually occurs at the tip of the crack, will directly affect the productivity of oil and gas wells (Li et al., 2022; Bessmertnykhet al., 2020). This phenomenon is also found in the injecting test in this study. Except that some proppants are fixed due to the confining pressure, other proppants are transported freely in the fracture. With the progress of test, proppant deposits incrementally at the end of the fluid flow path, as shown in Fig 10. It is obvious that the most serious proppant accumulation at the fracture bottom occurs under the condition of P0.1 and no proppant even plays a supporting role in the fluid flow path, as shown in Fig 10a. The proppant clumping is detected at the ends of the fluid flow path and this results in a decrease of the hydraulic conductivity.

Whereas, under conditions of P0.5 and P1.0, proppants in the fluid flow path can be divided into two categories according to the depositional modes: proppants fixed in the middle section of the fluid flow path due to partial sealing and plugging agent at the end of fracture. It may have a contradictory effect on fracture water conductivity. In this situation, the hydraulic aperture of fractures depends on the particle size of the proppants which are fixed in the middle of the fracture and the degree of proppant accumulation.

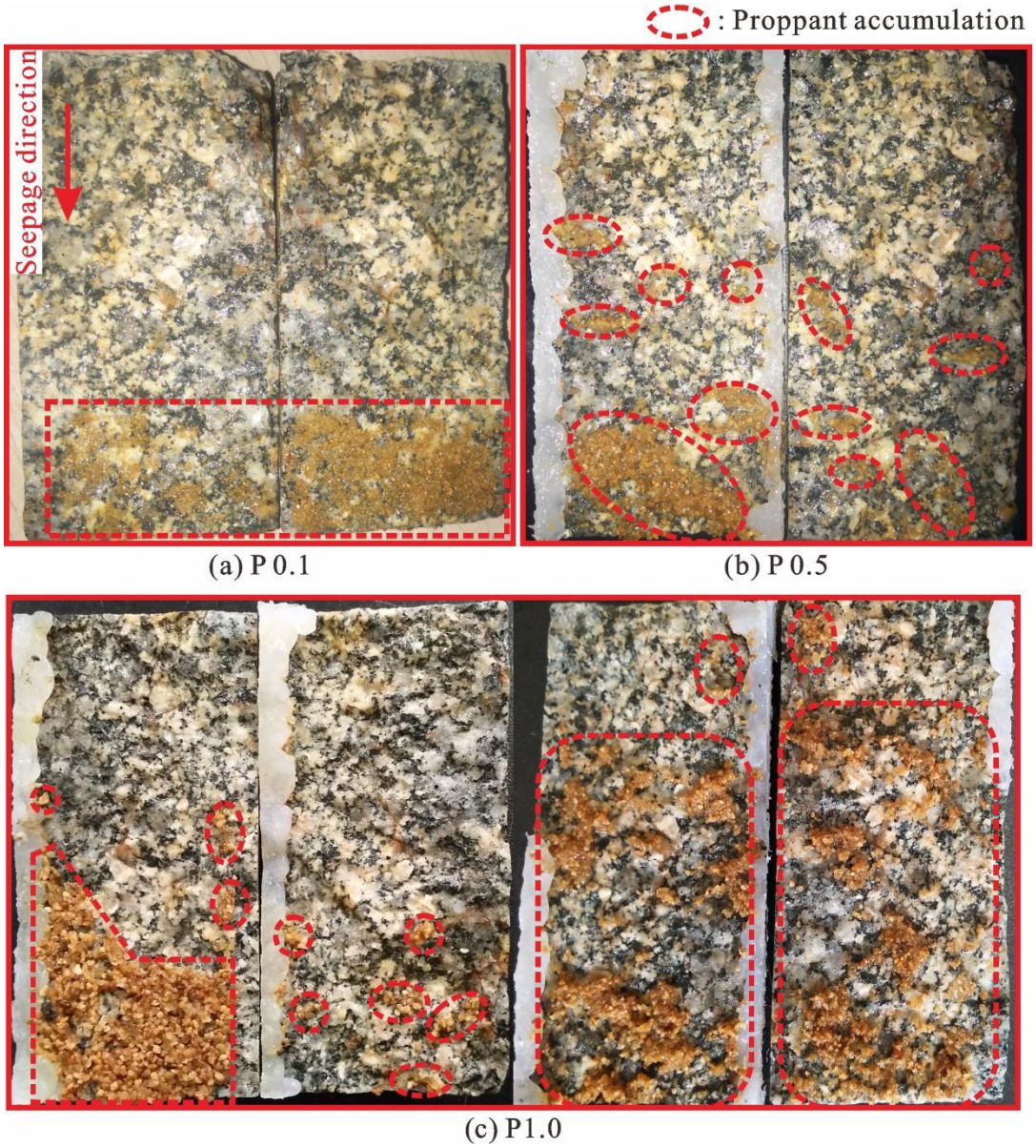

Figure 10: Proppant distribution in fracture after the hydraulic properties test

In order to further explore the influence of proppant accumulation level on fracture permeability, we divide the degree of proppant accumulation into four grades according to the distribution distance of proppant in the fluid flow path after the injecting test, as shown in Fig. 11. It can be seen that the equivalent hydraulic aperture (e) of fractures drops sharply as the proppant accumulation degree increases from I to IV. Meanwhile, we found that IV degree accumulation occurs under the condition of P0.1 and I degree accumulation occurs under the condition of P1.0 exclusively. Under any proppant conditions, proppant accumulation occurred at the end of the fluid flow path after the test. In the state, the hydraulic conductivity of fractures depends on the size of the intergranular pores of proppant. Meanwhile, undoubtedly, even if proppant accumulation occurs due to its free transport, there will always be proppants fixed by confining pressure which makes the fracture open and maintains high hydraulic conductivity when the proppants with the grain size of 0.5 mm and 1.0 mm are used. The above test results indicate that regardless of the grain size of the proppant, accumulation is inevitable in fractures during injecting. Therefore, compared with the P0.1, the larger intergranular space among proppant with the grain size of 1.0 mm can offset the reduction in hydraulic conductivity by proppant accumulation.

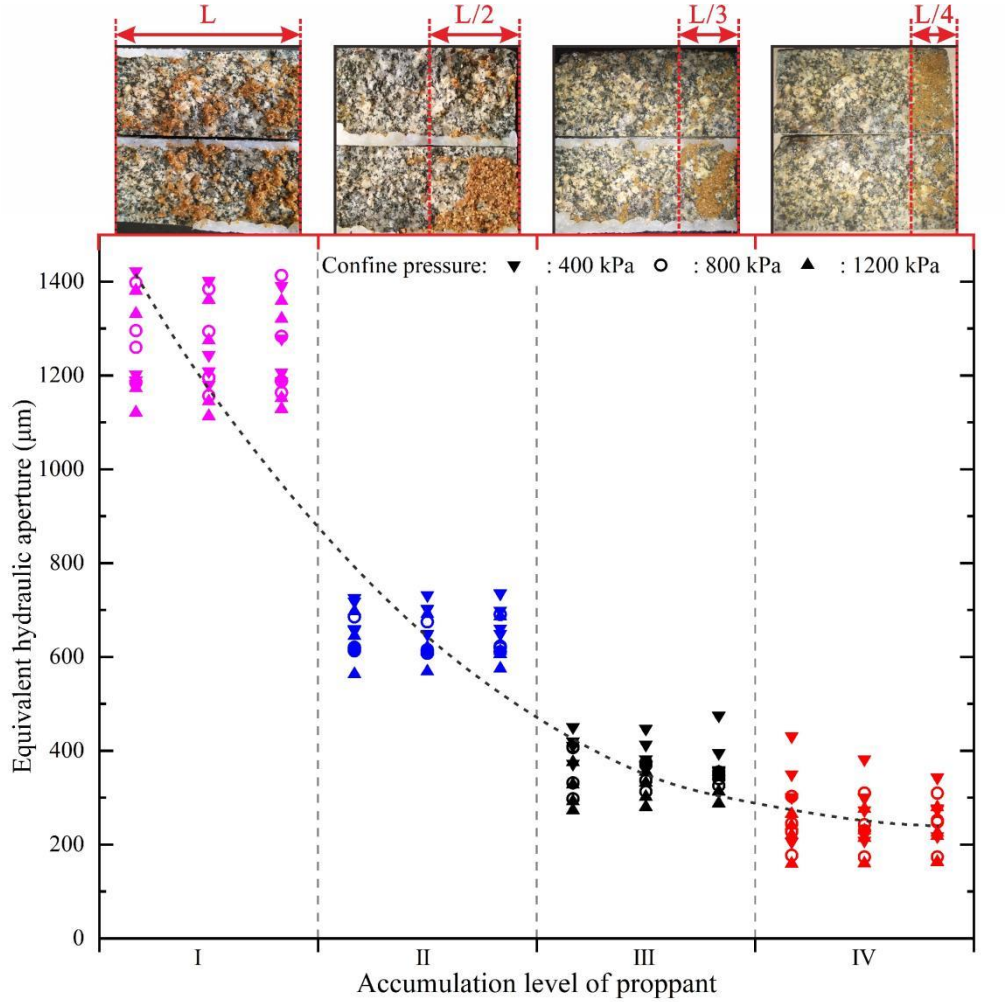

Figure 11: The equivalent hydraulic aperture of fractures monitored by fracture injecting test under four accumulation levels of proppant

3.5 The hydraulic properties with different proppant density

The above test results indicate that regardless of the particle size of the proppant, accumulation is inevitable in fractures during injecting. In order to reveal the evolution of fracture permeability under proppant accumulation, we studied the effect of proppant distribution density on hydraulic properties. The total amount of proppant on the fracture surface is controlled to ensure that its distribution density remains at three levels of 10/cm^2, 20/cm^2 and 30/cm^2, and the pressure condition is controlled at 300 kPa of pore pressure and 1200 kPa of confine pressure. The results show that with the increase of proppant distribution density, the hydraulic conductivity of P0.1 decreases sharply, as shown in Fig. 12. When the density reaches 30/cm^2, the hydraulic conductivity is only 23% of 10/cm^2. However, when the proppant particle size reaches 1 mm, the hydraulic conductivity decreases slightly with the increase of distribution density, only 6% average. Therefore, compared with the P0.1, the larger intergranular space in P1.0 can offset the reduction in hydraulic conductivity by proppant accumulation. It can be concluded that, in order to alleviate the low hydraulic conductivity of EGS production wells caused by proppant blockage, a coarse grain size of proppant is expected to be with high potential in application in HDR reservoir stimulation.

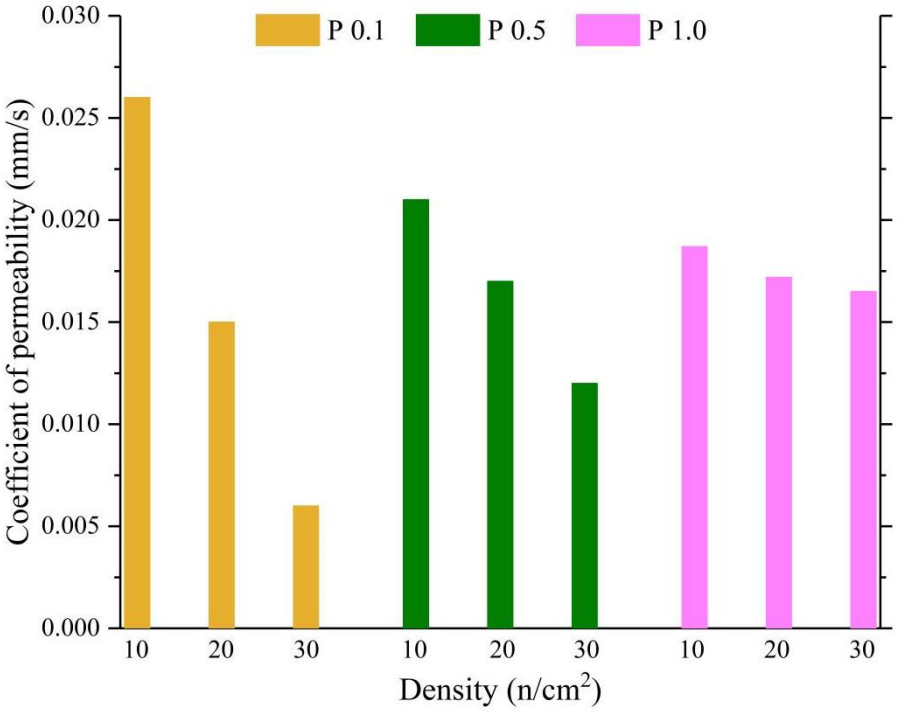

Figure 12: The relationship between hydraulic conductivity (K_j) with distribution density of proppant in fractures

.4. DISCUSSION

4.1 Hydraulic conductivity

Under the coupling effect of shear stimulation and aperture propping, the optimization effect to fracture permeability obtained by theoretical calculation in Table 3 is higher than the test results. This is because the accumulation effect of proppants and asperities are not considered in the theoretical calculation, which is undesirable in the actual reservoir stimulation behavior. When large grain size proppants are used, the phenomenon of proppant blockage is alleviated due to the intergranular pore, as shown in Fig. 13b. This effect needs to be considered for effective shear stimulation. Moreover, even though proppant placement can increase the fracture aperture, the propped fracture also experiences less shear dilation, especially at large shear displacement.

4.2 Fractures roughness

Shear dilation due to surface roughness, also called self-propping, can keep fractures open (Brace, 1980; Durham & Bonner, 1994). However, under the ultra-high in-situ stress conditions in the HDR reservoir, the fracture surfaces with a high shear strength are damaged acutely in the process of shear stimulation and the self-supporting aperture filled directly by granite debris, which may directly lead to the target stimulation reservoir's unminable, as shown in Fig. 13a. For the propped fractures, however, the surface roughness analysis showed that the fractures experienced insignificant damage. This suggests that proppant, with the role of lubricant, protected the asperities by preventing their interlocking and interactions. The crushing of moiety proppants controlled by local stress replaces the fragmentation of rock debris, as shown in Fig. 13b. It makes the self-supporting dilatancy of fractures easier and generates a positive impact on hydraulic conductivity. Moreover, the results of direct shear test we obtained in this study are from fractures with different roughness. The fact that we observe the transition of frictional behavior under different proppant conditions indicates that these are systematic first-order dependencies that override the impacts of the specific variabilities in fracture roughness. These observations suggest that there is an interplay among the influences of fracture surface roughness, proppant conditions, and normal stress. Understanding this relationship may be the key to optimizing the hydraulic permeability in reservoir stimulation.

4.3 Proppant accumulation

Our research has proved that proppants could be accumulated in fractures when the proppants are used to stimulate HDR reservoirs. And the fracture can maintain hydraulic conductivity well when the proppants with a coarse grain size are used. Hence, the grain size grading of the proppant needs to be carefully selected. When proppant accumulation occurs, the hydraulic conductivity of the fracture will no longer singly depend on the mechanical aperture of the fracture but will depend on the intergranular pores of the proppant, which is a gradual transformation process with the accumulation process. Hence, for a fractured reservoir, the ideal state is that the particle size grading of proppants needs to be fit with the opening of pre-existing fractures in the HDR reservoir so that proppants can be fixed in a proper position by confine pressure and will not be blocked due to free transportation to the end of the fluid flow path.

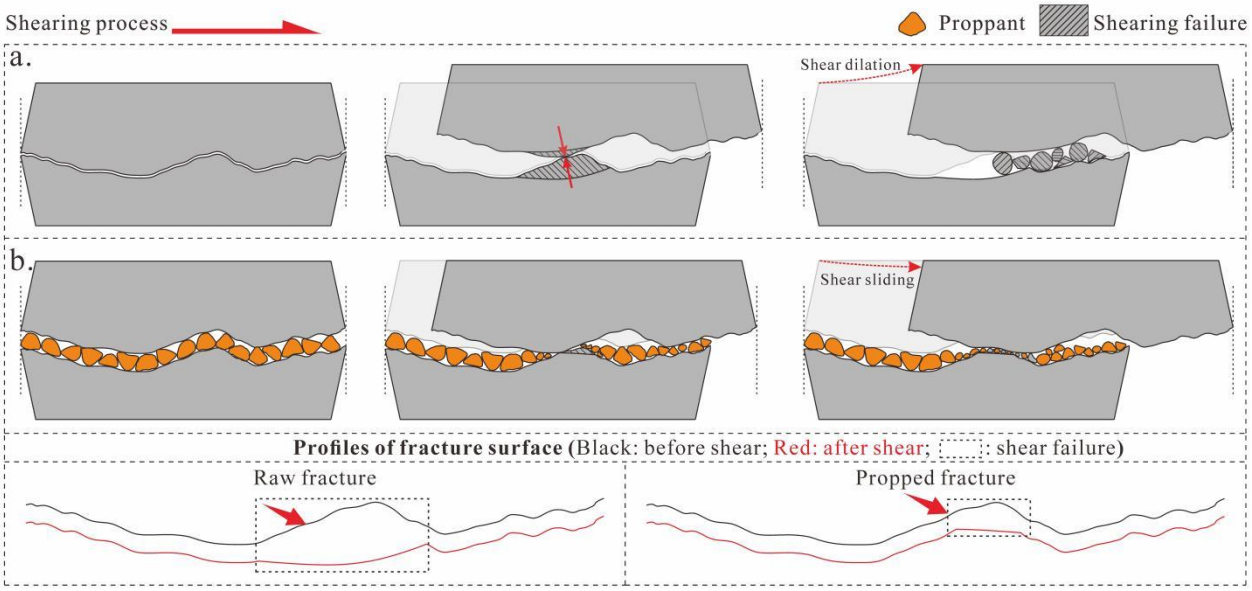

Figure 13: Schematic diagram to display the protective effect of proppant on fracture surface during the shear process. (a): raw fractured granite and (b): propped fractured granite

5. CONCLUSION

In this paper, the shear process of propped fractures and its implications on the enhancement of hydraulic permeability are examined. The change of roughness features of the fracture surfaces before and after the shear test is studies to understand the effects of proppant on the altering the surface geometry of propped fractures. The major findings obtained from this study are:

- To investigate the effects of proppant on the hydraulic properties of fractured granite, the fracture injecting test is carried out under constant confining pressure and pore pressure. By placing the proppant with a density of 10/cm^2 in the fracture, the equivalent hydraulic aperture increases from 119.79 μm to 1192.07 μm and the average hydraulic conductivity increases from 0.013 mm/s to 1.150 mm/s with increasing the proppant grain size from P0.0 to P1.0. Furthermore, compared with the P0.1, the larger intergranular space among proppant of P1.0 can offset the reduction in hydraulic conductivity by proppant accumulation.

- Shear dilation is is highly affected by the grain size of proppant, compared with the shear dilation of P0.0 with a dilatancy rate of 0.123 mm/mm, the samples with proppant show a lower vertical dilation (average 0.095) during the shearing process. In addition, the larger the grain size of proppant, the longer the sliding displacement is. By coupling both effects of proppants and shear dilation, the samples with larger proppant sizes achieve higher vertical displacement, indicating a higher hydraulic aperture. The hydraulic permeability of fractured granite is effectively increased by 1600 times by placing proppant of P1.0.

- An analysis of roughness features before and after shear stimulation shows a slighter change in surface roughness when the fracture is propped compared with the raw samples. The highest reduction of roughness, the △JRC, is -11.36 in the raw sample and the remarkably lower △JRC (average -1.47) is detected when the fracture is propped. This could be attributed to the proppant protecting the asperities damage by preventing their interlocking and interactions, and the crushing of moiety proppants compressed by local stress replaces the fragmentation of rock debris, so as to relieve the shear failure of fracture surfaces. The roughness of fracture is a key to a success of a shear stimulation. The lower the reduction of surface roughness is, the higher the hydraulic stimulation can be expected. Thus, the placing of proppant in a shear stimulation to protect the degradation of surface roughness is a useful approach to enhance hydraulic permeability of a reservoir.

The proppant clumping is detected at the ends of the fluid flow path which has a low hydraulic head and this results in a decrease of the hydraulic conductivity in our particular tests with the narrow flow path. The fracture propped by P0.5 and P1.0 can maintain a favorable high hydraulic conductivity due to the propping effects. In practice, since the flow path is much wider, the proppants may enter into the edges of the fractures where has relatively low fluid pressure and this undesirable proppant accumulation can be mitigated due to the scale effects in practical engineering.

REFERENCES

Zhu, J., Hu, K., Lu, X., Huang, X., Liu, K., Wu, X.: A review of geothermal energy resources, development, and applications in China: Current status and prospects. Energy, 93, (2015), 466-483.

Sun, Z.X., Zhang, X., Xu, Y., Yao, J., Wang, H.X., Lv, S., Sun, Z., Huang, Y., Cai, M., Huang, X.: Numerical simulation of the heat extraction in EGS with thermal-hydraulic-mechanical coupling method based on discrete fractures model. Energy, 120, (2017), 20-33.

Lu, S. M.: A global review of enhanced geothermal system (EGS). Renewable and Sustainable Energy Reviews, 81, (2018), 2902-2921.

Luo, J., Zhu, Y., Guo, Q., Tan, L., Zhuang, Y., Liu, M., Zhang, C., Zhu, M., Xiang, W.: Chemical stimulation on the hydraulic properties of artificially fractured granite for enhanced geothermal system. Energy, 142, (2018), 754–764.

Chen, J., Jiang, F.: Designing multi-well layout for enhanced geothermal system to better exploit hot dry rock geothermal energy. Renewable Energy, 74, (2015), 37-48.

Huang, Z., Zhang, S., Yang, R., Wu, X., Li, R., Zhang, H., Hung, P.: A review of liquid nitrogen fracturing technology. Fuel, 266, (2020), 117040.

Zhu, G.P., Yao, J., Sun, H., Zhang, M., Xie, M.J., Sun, Z.X., Lu, T.: The numerical simulation of thermal recovery based on hydraulic fracture heating technology in shale gas reservoir. Journal of Natural Gas Science and Engineering, 28, (2016), 305-316.

Zeng, Y.C., Su, Z., Wu, N.Y.: Numerical simulation of heat production potential from hot dry rock by water circulating through two horizontal wells at Desert Peak geothermal field. Energy, 56, (2013), 92-107.

Olasolo, P., Juárez, M.C., Morales, M.P., Liarte, I.A.: Enhanced geothermal systems (EGS): A review. Renewable and Sustainable Energy Reviews, 56, (2016), 133-144.

Gong, Y., Mehana, M., El-Monier, I., Viswanathan, H.: Proppant placement in complex fracture geometries: A computational fluid dynamics study. Journal of Natural Gas Science and Engineering, 79, (2020), 103295.

Aslannezhad, M., Kalantariasl, A., You, Z., Iglauer, S., Keshavarz, A.: Micro-proppant placement in hydraulic and natural fracture stimulation in unconventional reservoirs: A review. Energy Reports, 7, (2021), 8997-9022.

Chen, T., Fu, Y., Feng, X.T., Tan, Y., Cui, G., Elsworth, D., Pan, Z.: Gas permeability and fracture compressibility for proppant-supported shale fractures under high stress. Journal of Natural Gas Science and Engineering, 95, (2021), 104157.

Tan, Y., Pan, Z., Liu, J., Feng, X.T., Connell, L.D.: Laboratory study of proppant on shale fracture permeability and compressibility. Fuel, 222, (2018), 83-97.

Wang, J., Huang, Y., Zhou, F., Liang, X.: The influence of proppant breakage, embedding, and particle migration on fracture conductivity. Journal of Petroleum Science and Engineering, 193, (2020), 107385.

Zhong, Y., Kuru, E., Zhang, H., Kuang, J., She, J.: Effect of fracturing fluid/shale rock interaction on the rock physical and mechanical properties, the proppant embedment depth and the fracture conductivity. Rock Mechanics and Rock Engineering, 52(4), (2019), 1011-1022.

Isah, A., Hiba, M., Al-Azani, K., Aljawad, M.S., Mahmoud, M.: A comprehensive review of proppant transport in fractured reservoirs: Experimental, numerical, and field aspects. Journal of Natural Gas Science and Engineering, 88, (2021), 103832.

Barboza, B.R., Chen, B., Li, C.: A review on proppant transport modelling. Journal of Petroleum Science and Engineering, 204, (2021), 108753.

Ghassemi, A.: A review of some rock mechanics issues in geothermal reservoir development. Geotechnical and Geological Engineering, 30(3), (2012), 647-664.

Ye, Z., Ghassemi, A.: Injection-induced shear slip and permeability enhancement in granite fractures. Journal of Geophysical Research: Solid Earth, 123(10), (2018a), 9009-9032.

Bijay, K.C., Ghazanfari, E.: Geothermal reservoir stimulation through hydro-shearing: an experimental study under conditions close to enhanced geothermal systems. Geothermics, 96, (2021), 102200.

Guglielmi, Y., Cappa, F., Avouac, J.P., Henry, P., Elsworth, D.: Seismicity triggered by fluid injection-induced aseismic slip. Science, 348(6240), (2015), 1224–1226.

Guglielmi, Y., Elsworth, D., Cappa, F., Henry, P., Gout, C., Dick, P. et al.: In situ observations on the coupling between hydraulic diffusivity and displacements during fault reactivation in shales. Journal of Geophysical Research: Solid Earth, 120, (2015), 7729–7748.

Ye, Z., Ghassemi, A.: Experimental study on injection-induced fracture propagation and coalescence for EGS stimulation. Paper presented at the 43rd Workshop on Geothermal Reservoir Engineering, Stanford, CA, (2018b).

Huang, K., Zhang, Z., Ghassemi, A.: Modeling three-dimensional hydraulic fracture propagation using virtual multidimensional internal bonds. International Journal for Numerical and Analytical Methods in Geomechanics, 37(13), (2013), 2021–2038.

Hofmann, H., Blöcher, G., Milsch, H., Babadagli, T., Zimmermann, G.: Transmissivity of aligned and displaced tensile fractures in granitic rocks during cyclic loading. International Journal of Rock Mechanics and Mining Sciences, 87, (2016), 69–84.

Ishibashi, T., Asanuma, H., Fang, Y., Wang, C., Elsworth, D.: Exploring the link between permeability and strength evolution during fracture shearing. Paper presented at the 50th U.S. Rock Mechanics/Geomechanics Symposium, Houston, TX, (2016). https://doi.org/10.1016/j.foodres.2016.09.012

Vogler, D., Amann, F., Bayer, P., Elsworth, D.: Permeability evolution in natural fractures subject to cyclic loading and gouge formation. Rock Mechanics and Rock Engineering, 49(9), (2016), 3463–3479.

Liu, J.S. Seepage formula of single fracture under normal stress. Hydrogeology and Engineering Geology, 2, (1987), 32-33.

Xiong, X.B., Zhang, C.H., Wang, E.Z.: A review of steady state seepage in a single fracture of rock. Chinese Journal of Rock Mechanics and Engineering, 28(9), (2009), 1839-1847.

Witherspoon, P.A., Wang, J.S., Iwai, K., Gale, J.E.: Validity of cubic law for fluid flow in a deformable rock fracture. Water resources research, 16(6), (1980), 1016-1024.

Wang, Y.: Coupling characteristic of stress and fluid flow within a single fracture. Chinese Journal of Rock Mechanics and Engineering, 21(1), (2002), 83-87.

Tsang, Y.W., Witherspoon, P.A.: The dependence of fracture mechanical and fluid flow properties on fracture roughness and sample size. Journal of Geophysical Research: Solid Earth, 88(B3), (1983), 2359-2366.

Magsipoc, E., Zhao, Q., Grasselli, G.: 2D and 3D Roughness Characterization. Rock Mechanics and Rock Engineering, 53(3), (2020), 1495–1519.

Tse R, Cruden DM.: Estimating joint roughness coefficients. International journal of rock mechanics and mining sciences & geomechanics abstracts. Pergamon, 16(5) (1979): 303-307.

Myers, N.O. Characterization of surface roughness. Wear, 5(3), (1962), 182-189.

Sayles, R.S., Thomas, T.R.: The spatial representation of surface roughness by means of the structure function: a practical alternative to correlation. Wear, 42(2), (1977), 263-276.

Yang, Z.Y., Lo, S.C., Di, C.C.: Reassessing the joint roughness coefficient (JRC) estimation using Z2. Rock mechanics and rock engineering, 34(3), (2001), 243-251.

Olssona, R., Barton, N.: An improved model for hydromechanical coupling during shearing of rock joints. International Journal of Rock Mechanics & Mining Sciences, 38, (2001), 317–329.

Brace, W.F.: Permeability of crystalline and argillaceous rocks. International Journal of Rock Mechanics and Mining Sciences & Geomechanics Abstracts, 17(5), (1980), 241-251.

Durham, W.B., Bonner, B.P.: Self-propping and fluid flow in slightly offset joints at high effective pressures. Journal of Geophysical Research: Solid Earth, 99(B5), (1994), 9391-9399.

Luo, J., Zhu, Y., Guo, Q., Tan, L., Zhuang, Y., Liu, M., Zhang, C., Xiang, W., Rohn, J.: Experimental investigation of the hydraulic and heat-transfer properties of artificially fractured granite. Scientific Reports, 7,(2017), 39882.

Shi, Z.M., Shen, D.Y., Zhang, Q.Z., Peng, M., Li, Q.D.: Experimental study on the coupled shear flow behavior of jointed rock samples. European Journal of Environmental and Civil Engineering, (22), (2017), 1–18.

Li, J., Wei, J., Zhou, X., Zhang, A., Yang, Y., Wang, A., ... & Rong, G.: Influence of proppant physical properties on sand accumulation in hydraulic fractures. Journal of Petroleum Exploration and Production Technology, 12(6), (2022), 1625-1632.

Bessmertnykh, A., Dontsov, E., Ballarini, R.: The effects of proppant on the near-front behavior of a hydraulic fracture. Engineering Fracture Mechanics, 235, (2020), 107110.